



Staphylococcal Bacterial Persister Cells, Biofilms, and Intracellular Infection Are Disrupted by JD1, a Membrane-Damaging Small Molecule

Jamie L. Dombach,^a Joaquin L. J. Quintana,^a  Corrella S. Detweiler^a

^aDepartment of Molecular, Cellular, and Developmental Biology, University of Colorado Boulder, Boulder, Colorado, USA

ABSTRACT Rates of antibiotic and multidrug resistance are rapidly rising, leaving fewer options for successful treatment of bacterial infections. In addition to acquiring genetic resistance, many pathogens form persister cells, form biofilms, and/or cause intracellular infections that enable bacteria to withstand antibiotic treatment and serve as a source of recurring infections. JD1 is a small molecule previously shown to kill Gram-negative bacteria under conditions where the outer membrane and/or efflux pumps are disrupted. We show here that JD1 rapidly disrupts membrane potential and kills Gram-positive bacteria. Further investigation revealed that treatment with JD1 disrupts membrane barrier function and causes aberrant membranous structures to form. Additionally, exposure to JD1 reduced the number of *Staphylococcus aureus* and *Staphylococcus epidermidis* viable persister cells within broth culture by up to 1,000-fold and reduced the matrix and cell volume of biofilms that had been established for 24 h. Finally, we show that JD1 reduced the number of recoverable methicillin-resistant *S. aureus* organisms from infected cells. These observations indicate that JD1 inhibits staphylococcal cells in difficult-to-treat growth stages as well as, or better than, current clinical antibiotics. Thus, JD1 shows the importance of testing compounds under conditions that are relevant to infection, demonstrates the utility that membrane-targeting compounds have against multidrug-resistant bacteria, and indicates that small molecules that target bacterial cell membranes may serve as potent broad-spectrum antibacterials.

IMPORTANCE Untreatable bacterial infections are a critical public health care issue. In addition to increasing antibiotic resistance, bacteria that are in slow-growing or non-growing states, or that live inside mammalian cells, are typically insensitive to clinical antibiotics and therefore difficult to eradicate. Bacterial cell membranes have been proposed as potential novel antibiotic targets that may be vulnerable in these difficult to treat cell types because cell membranes are always present and performing essential functions. The small molecule JD1 was previously shown to disrupt Gram-negative bacterial cell membranes. Here, we show that it also disrupts the cell membrane of Gram-positive bacteria and reduces viable bacteria within persister populations, biofilms, and mammalian cells. These observations demonstrate the importance of testing novel compounds under infection-relevant conditions, because their potency against rapidly growing cells may not reveal their full potential.

KEYWORDS Gram-positive bacteria, membrane structure, *Staphylococcus*, biofilms, persister cells, intracellular infection, *Salmonella*, antibacterial, bactericidal activity, cell membranes, Gram-negative bacteria, intracellular pathogen, membrane potential, outer membrane

Few new antibiotics with novel structures or functions have been approved for use over the last several decades, limiting the treatment options for bacterial infections (1). In addition, since many existing antibiotics bind the same target in similar

Citation Dombach JL, Quintana LJ, Detweiler CS. 2021. Staphylococcal bacterial persister cells, biofilms, and intracellular infection are disrupted by JD1, a membrane-damaging small molecule. *mBio* 12:e01801-21. <https://doi.org/10.1128/mBio.01801-21>.

Editor Michele S. Swanson, University of Michigan—Ann Arbor

Copyright © 2021 Dombach et al. This is an open-access article distributed under the terms of the [Creative Commons Attribution 4.0 International license](https://creativecommons.org/licenses/by/4.0/).

Address correspondence to Jamie L. Dombach, jamie.dombach@colorado.edu, or Corrella S. Detweiler, detweile@colorado.edu.

Received 21 June 2021

Accepted 13 September 2021

Published 12 October 2021

locations, resistance to one antibiotic quickly enables cross-resistance to multiple antibiotics, notably for macrolides, lincosamides, and streptogramins and for β -lactams (2). Due to the rapid development of resistance, the few antibiotics that are effective against multidrug-resistant (MDR) bacteria are reserved for use in critical cases. These antibiotics are referred to as last line of defense or last resort antibiotics and often have severe side effects that limit their utility (3, 4).

The increase in antibiotic resistance is occurring in both Gram-positive and Gram-negative bacteria, which use common cellular mechanisms, growth stages, and infection strategies to evade antibiotics and host immunity. For instance, toxic molecules, including antibiotics, are exported by efflux pumps. However, Gram-negative bacteria are especially difficult to kill due to their outer membrane, which blocks many compounds from entering the cell (5). These bacteria primarily use efflux pumps of the resistance-nodulation-division (RND) family to export antibiotics (6, 7). In addition to expelling antibiotics, efflux pumps have an important role during infection, as they export host-derived molecules that would otherwise damage the bacterial cell, including the Gram-negative outer membrane (8, 9).

Shared mechanisms of host evasion include the establishment of a persister state, biofilms, and an intracellular lifestyle. Bacterial persister cells may be defined as non-growing and/or metabolically less active cells that constitute a small population in all cultures of bacteria but can increase in proportion (10). For example, 100% of *Staphylococcus* cultures become persister cells with growth at high density. When environmental conditions become favorable, persister cells exit their metabolically quiescent state and resume active growth (11–14). Their decreased metabolism protects persister cells from most currently available antibiotics, which interfere with processes that only occur, or occur more rapidly, in metabolically active or actively growing cells (15). Due to their intrinsically high resistance to antibiotics, persisters are an important cause of recurring infections (15). Persister cells also reside within biofilms and may reside intracellularly during infection. Biofilms are notoriously difficult to treat due to an extracellular matrix that excludes many compounds, including antibiotics (12, 16). The biofilms of *Staphylococcus epidermidis* are particularly robust and grow on medical implants (16, 17). In contrast, *Staphylococcus aureus* resides both extracellularly and intracellularly during infection (18, 19). Intracellular pathogens evade neutralizing components of the host immune system such as antibodies and neutrophils, allowing them refuge in a protected environment (20, 21). Additionally, intracellular pathogens may cause recurring infections by escaping antibiotic treatment, as concentrations of antibiotics tend to be lower inside host cells than in the extracellular environment (22).

Compounds with activity against the bacterial cell membrane may be effective for treating cells in a persister state, in biofilms, and within host cells, because at all times the cell membrane is essential (23–26). The lipid composition of bacterial cell membranes is distinct from that of mammalian cell membranes and is mainly composed of phosphatidylethanolamine (PE), phosphatidylglycerol, and cardiolipin, although there are differences in membrane composition across bacteria. For instance, glucolipids are a feature of Gram-positive bacteria (27), and *S. aureus* has very little PE (28). Nevertheless, bacterial cell membranes have a more negative overall charge than mammalian cell membranes, which are mainly composed of phosphatidylcholine, PE, phosphatidylserine, and cholesterol (25, 29). The outer leaflet of mammalian cell membranes has a more overall neutral charge, in part because negatively charged lipids tend to be within the inner leaflet (25). These distinctions indicate that small molecules that preferentially target bacterial membranes over mammalian membranes may exist.

JD1 (406 g/mol) is a small aromatic molecule that facilitates the killing of the Gram-negative pathogen *Salmonella enterica* serovar Typhimurium in mammalian macrophages and epithelial cells and reduces bacterial load in mice. In broth culture, JD1 damages the inner membrane if conditions permeabilize the outer membrane and/or the RND family AcrAB-TolC efflux pump is inactivated (30). We therefore examined the effect of JD1 on Gram-positive bacteria, which lack an outer membrane and may

TABLE 1 Concentrations of JD1 that inhibit Gram-positive bacterial growth

| Strain | JD1 MIC ₅₀ (μM) | JD1 cMIC ₉₅ ^a | |
|------------------------------|----------------------------|-------------------------------------|-------|
| | | μM | μg/ml |
| <i>B. subtilis</i> ATCC 6633 | 10.6 ± 6.3 | 12.5 | 5.1 |
| <i>S. aureus</i> Newman | 35.6 ± 0.5 | 40.2 | 16.4 |
| <i>S. aureus</i> FDA209 | 26.5 ± 1.0 | 29.7 | 12.1 |
| <i>S. aureus</i> USA300 | 29.1 ± 2 | 41.0 | 16.7 |
| <i>S. aureus</i> HG001 | 33.2 ± 4.5 | 49.0 | 19.9 |
| <i>S. epidermidis</i> 1457 | 21.6 ± 2.7 | 30.8 | 12.5 |

^acMIC₉₅ is the calculated MIC₉₅.

facilitate JD1 access to the cell membrane in persister cells and biofilms. We began with traditional laboratory model organisms (*Bacillus subtilis* and *S. aureus* Newman) and progressed to more virulent strains. *Staphylococcus* species tested included *S. aureus* and *S. epidermidis*, both of which form persister cells and biofilms, but only *S. aureus* causes intracellular infections. *S. aureus* FDA209 was isolated from a skin lesion, is sensitive to antibiotics, and has historically been used in antimicrobial and quality control testing (31–33). *S. aureus* HG001 is a common lab strain derivative of NCTC835, a methicillin-sensitive strain isolated from a septic patient but with a restored *rsbU*⁺ gene to increase its biofilm production (34). *S. aureus* USA300 grows rapidly and is a community-acquired methicillin-resistant strain that causes intracellular infections (35). Finally, we examined *S. epidermidis* 1457, which is antibiotic sensitive and forms robust biofilms (36).

Here, we show that JD1 disrupts the staphylococcal cell membrane and interrupts growth states that are critical to infections. Through the use of fluorescent probes, we found that JD1 increases the curvature and/or the fluidity of the cellular membrane of *S. aureus* and leads to a breakdown of barrier function. Using superresolution structured illumination microscopy (SR-SIM) and transmission electron microscopy (TEM), we also found that JD1 treatment results in the formation of membrane distortions. JD1 decreased the number of viable persister cells in broth, reduced established staphylococcal biofilms, and decreased the number of recoverable bacteria from intracellular infections. These data show the importance of testing novel compounds not just in broth culture but also in growth stages germane to infection and suggest that small, membrane-active molecules may serve as potent broad-spectrum antibacterials.

RESULTS

JD1 is bacteriostatic and bactericidal against Gram-positive bacteria. We established whether JD1 is potent against Gram-positive bacteria in standard broth compared to dimethyl sulfoxide (DMSO) (solvent control). When *Bacillus subtilis* (ATCC 6633) was grown in a rich medium (LB), JD1 inhibited growth with a MIC₉₅ of 12.5 μM. The MIC₉₅ is defined as the concentration required to inhibit 95% of bacterial growth after 18 h. Under the same conditions, the MIC₉₅s for *S. aureus* and *S. epidermidis* were 2- to 4-fold higher (Table 1 and Fig. 1A). In *S. Typhimurium*, MIC₉₅s ranged from 14 to 90 μM, depending on the conditions used to compromise the outer membrane (30). These data indicate that JD1 is similarly effective against Gram-positive bacteria and against Gram-negative bacteria that have sustained outer membrane damage.

To determine whether JD1 is bactericidal, we monitored optical density at 600 nm (OD₆₀₀) and recovery of CFU in cultures of *B. subtilis* and *S. aureus* FDA209 exposed to various concentrations of JD1 (Fig. 1B to E). Within 15 min of treatment at 2 × MIC₉₅, JD1 reduced the survival of *B. subtilis* and *S. aureus* by at least 10-fold and continued to kill cells over the next 2 h. Thus, JD1 is bactericidal for two distinct genera of Gram-positive organisms. While the *B. subtilis* laboratory strain was more sensitive to JD1 than the pathogenic *S. aureus* strains, further experiments were carried out with *S. aureus* due to the propensity of these strains to establish a persister state, form biofilms, and/or replicate within mammalian cells.

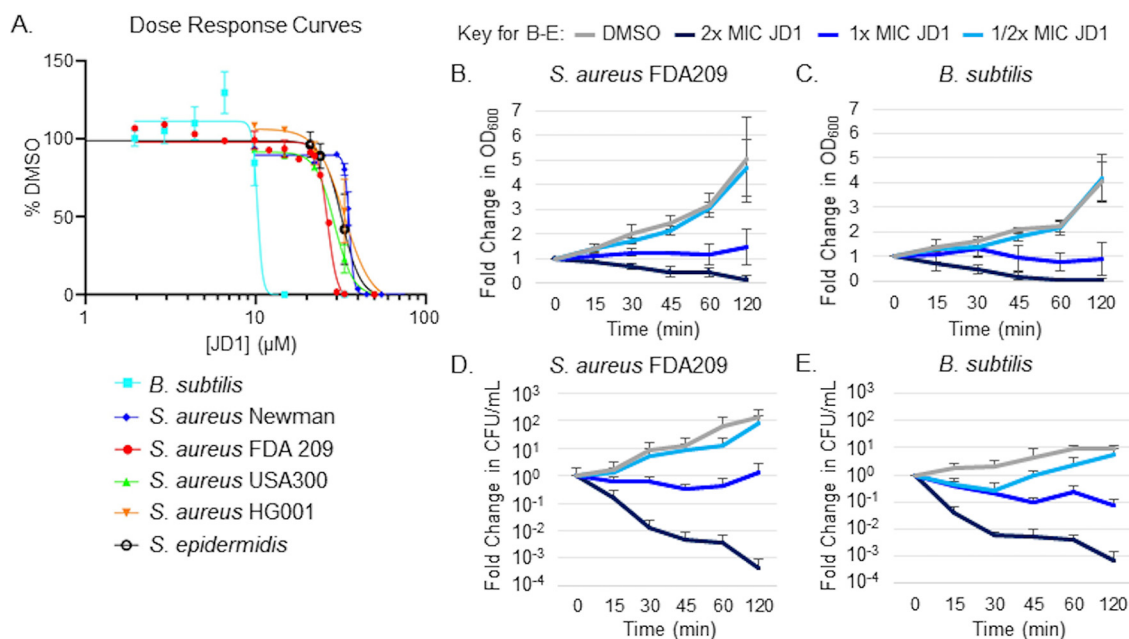


FIG 1 JD1 is bacteriostatic and bactericidal against Gram-positive bacteria. (A) Dose-response curves monitoring bacterial growth of the indicated strains from an OD_{600} of 0.01 in LB, normalized to growth in 2% DMSO. Means and standard errors of the means (SEM) for at least three biological replicates performed with technical triplicates are shown. (B to E) Growth curves and kill curves. Mid-log-phase LB-grown cultures of the indicated strains were treated at time zero with either DMSO or the corresponding MIC_{95} of JD1 (Table 1). Cultures were monitored for OD_{600} (B and C) and plated for enumeration of CFU (D and E). Data are presented as fold change. Means and SEM for three biological replicates performed with technical triplicates are shown.

The membrane potential of *S. aureus* is rapidly disrupted upon JD1 treatment.

JD1 immediately disrupted the inner membrane and membrane potential of *S. Typhimurium* but much more slowly reduced respiration and ATP accumulation (30). To establish whether the compound acts similarly in *S. aureus*, cells were loaded with the fluorescent probe 3,3'-dipropylthiadicarbocyanine iodide [$DiSC_3(5)$], which accumulates within and is quenched by polarized cell membranes. $DiSC_3(5)$ becomes highly fluorescent upon release from the membrane (barrier disruption) or depolarization (ion gradients) (37, 38). As anticipated, treatment of *S. aureus* with gramicidin, a mixture of large (1,882-g/mol), pore-forming peptides that depolarizes membranes (39), increased $DiSC_3(5)$ fluorescence within minutes (Fig. 2A). When cells were treated with $2\times MIC_{95}$ JD1, an equally rapid and robust increase in fluorescence was observed. At lower doses, the response was slower and more modest. These results show that JD1 disrupts membrane function in *S. aureus*.

To test whether JD1 affects the pH gradient in *S. aureus*, we measured the intracellular H^+ concentration using the fluorescent probe BCECF-AM [2',7'-bis-(2-carboxyethyl)-5-(and -6)-carboxyfluorescein, acetoxymethyl ester] (40). While treatment with the protonophore carbonyl cyanide *m*-chlorophenyl hydrazone (CCCP) rapidly increased intracellular pH, cells treated with JD1 were indistinguishable from cells treated with DMSO (Fig. 2B), indicating that JD1 does not affect the pH gradient in *S. aureus*.

We used the indicator resazurin (41) to monitor respiration in *S. aureus* upon treatment with JD1. A significant decrease in reduction potential was observed only after 15 min in cells treated with $2\times MIC_{95}$ JD1 (Fig. 2C). Similarly, *S. aureus* exhibited a dose-dependent reduction in ATP levels when treated with $2\times MIC_{95}$ for 15 min (Fig. 2D). These data indicate that the decrease in reduction potential and in ATP levels is likely due to a secondary effect of JD1, suggesting that the primary mechanism of JD1-mediated cell death in *S. aureus* is membrane barrier disruption.

Treatment with JD1 perturbs *S. aureus* membrane barrier function and increases cell membrane fluidity. In Gram-negative bacteria, JD1 increased the permeability of the cell membrane to the DNA dye propidium iodide (PI). In *S. aureus*, we similarly

Key for A, B, F:

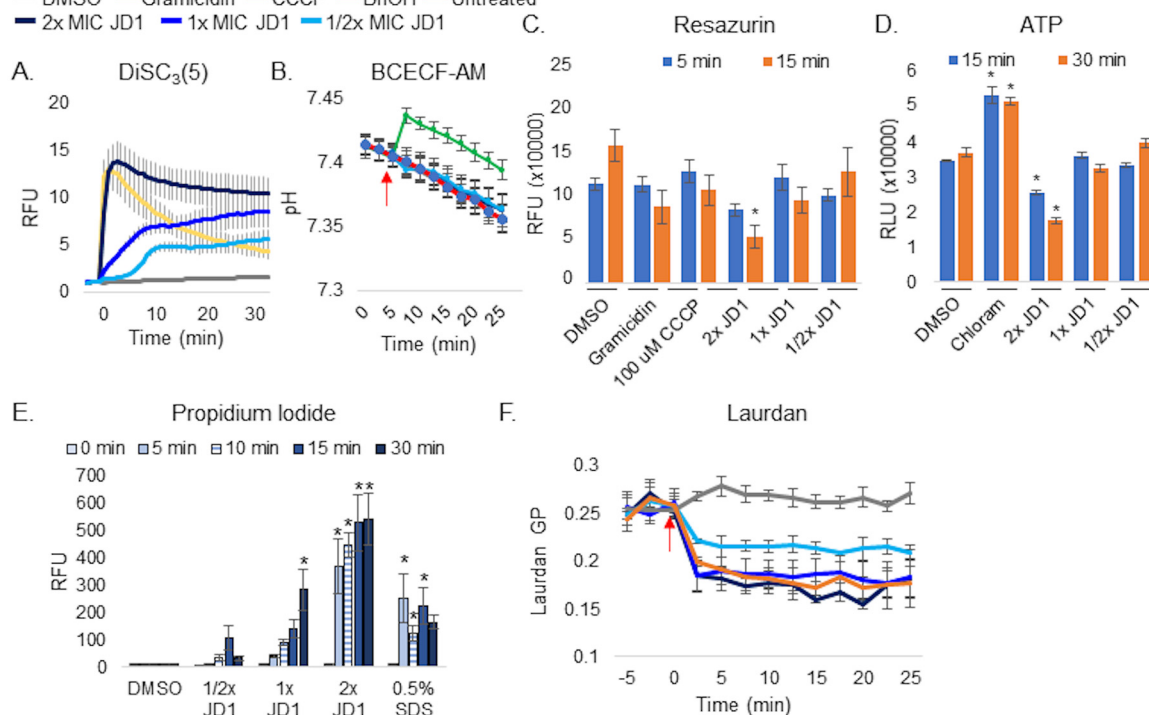
 — DMSO — Gramicidin — CCCP — BnOH — Untreated
 — 2x MIC JD1 — 1x MIC JD1 — 1/2x MIC JD1


FIG 2 JD1 damages the cytoplasmic membrane of *S. aureus* FDA209 and reduces laurdan GP without disrupting the pH gradient or respiration. JD1 MIC₉₅s are provided in Table 1. Mid-log-phase cells were used for all experiments. (A) Cell membrane potential was monitored with the fluorescent dye DiSC₃(5) in LB. Cells were treated at time zero with DMSO, gramicidin (2 μg/ml), or JD1. Means and SEM for three biological replicates performed with technical triplicates are shown. Data are normalized to DMSO at time zero. (B) Intracellular pH was monitored with the fluorescent probe BCECF-AM. Cells were treated with DMSO, the protonophore CCCP (100 μM), or JD1 at the time shown by the red arrow. Means and SEM for three biological replicates performed with technical triplicates are shown. (C) Respiration rates. Cells were incubated with resazurin and treated at time zero with DMSO, gramicidin (8 μg/ml), CCCP (100 μM), or JD1. Means and SEM for three biological replicates performed with technical triplicates are shown. (D) Intracellular ATP levels measured using the Promega BacTiter-Glo kit. Cells were treated for 15 or 30 min with DMSO, chloramphenicol (32 μg/ml), or JD1. Means and SEM for three biological replicates performed with technical triplicates are shown. (E) Cell membrane permeability was monitored by PI fluorescence. Cells were treated at time zero with DMSO, SDS (0.5%), or JD1. Samples were processed at the time points shown. Means and SEM for three biological replicates performed with technical triplicates are shown. (F) Laurdan GP. Cells were treated at the time indicated by the red arrow with DMSO, benzyl alcohol (BnOH) (50 mM), or JD1. Means and SEM for three biological replicates performed with technical triplicates are shown. All asterisks indicate a *P* value of ≤0.05 as determined by one-way analysis of variance (ANOVA) compared to DMSO at that time.

found that within 5 min of treatment with 2× MIC₉₅ JD1, or with the detergent SDS, there was a significant and dose dependent increase in PI fluorescence compared to DMSO (Fig. 2E). Thus, JD1 rapidly disrupts the barrier function of the cell membrane in *S. aureus*.

Defects in membrane barrier function may be caused by changes in membrane fluidity (42–44). Laurdan is a fluorescent probe that inserts into the phospholipid bilayer, and its emission spectrum changes with the polarity of its environment, as determined by calculating the generalized polarization (GP). As GP declines, membrane fluidity and/or curvature increases (45–47). Treatment with the membrane fluidizer benzyl alcohol (BnOH) rapidly decreased GP, as expected (48). Treatment with JD1 also decreased GP, in a dose-dependent manner (Fig. 2F). These data are consistent with a rapid JD1 effect that increases the fluidity and/or the curvature of the bacterial cell membrane.

Abnormal *S. aureus* membranous structures appear within minutes of JD1 treatment. Gram-negative bacteria treated with JD1 developed both internal and external membranous blebs, but whether they derived from the inner or outer membrane could not be determined. Since Gram-positive bacteria have only a single membrane, we performed a similar experiment with two *S. aureus* strains. Cells were treated with 1× MIC₉₅ JD1 and stained with the lipophilic dye Nile red and the DNA stain

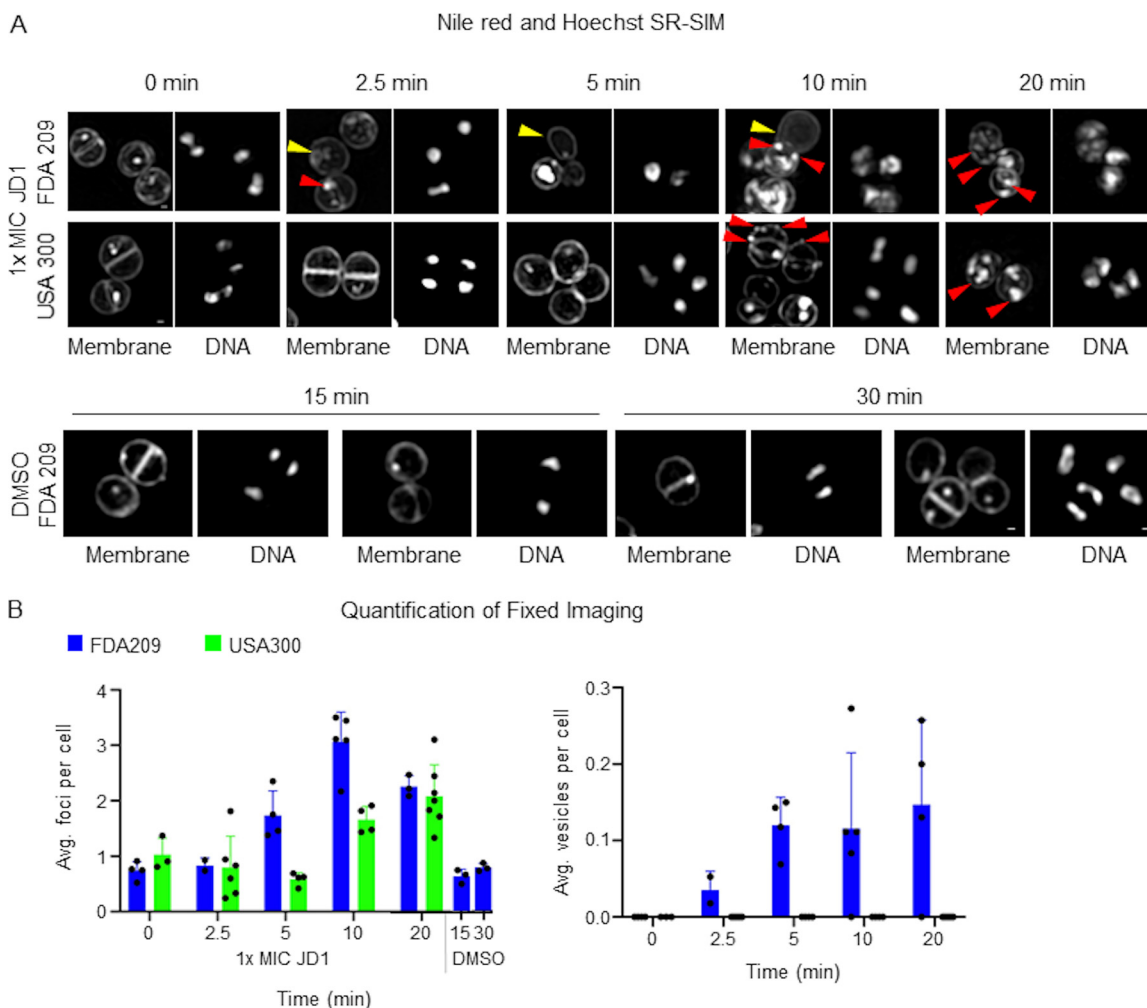


FIG 3 Multiple *S. aureus* cell membrane aberrations appear in response to JD1 treatment. (A) Nile red and Hoechst staining followed by SR-SIM imaging of *S. aureus* strains FDA209 and USA300. Cells were grown to mid-log phase, treated with $1 \times \text{MIC}_{95}$ JD1 (Table 1) or DMSO for the indicated period of time, stained with the lipophilic dye Nile red ($30 \mu\text{M}$) and the DNA dye Hoechst ($30 \mu\text{M}$), fixed, and imaged. Yellow arrowheads show examples of Nile red cell membrane blebs or circles inside and outside cells and lacking DNA. Red arrowheads indicate examples of Nile red puncta. Bar, 200 nm. Images are representative of two biological replicates, 2 to 7 fields of view, and 12 to 206 cells. (B) Quantification of aberrations seen in fixed-cell images of *S. aureus* cells treated with $1 \times \text{MIC}_{95}$ JD1 (Table 1) or DMSO. Each circle represents the number of puncta per cell in a field of view. Averages and standard deviations (SD) are shown.

Hoechst 33342. Live imaging suggested rapid membrane perturbation within minutes in the JD1-treated but not the DMSO-treated samples (Fig. S1). JD1 treatment increased the number of Nile red puncta 30-fold over DMSO treatment within 5 min. Fixed-cell imaging enabled higher resolution and revealed that within 2.5 min of treatment with JD1, *S. aureus* FDA209 cells had accumulated small, Nile red-stained intracellular membranous structures (Fig. 3, yellow arrowheads), and numerous distinct Nile red puncta around the membrane (red arrowheads). After 5 min of treatment, membranous protrusions appeared, apparently lacking DNA, and the number of Nile red puncta increased. Within 10 min, JD1-treated *S. aureus* acquired a large number of Nile red puncta (Fig. 3; Fig. S1). The accumulation of Nile red patches may represent areas of increased membrane fluidity and/or aberrant structural changes and show that JD1 alters the *S. aureus* cell membrane within minutes.

Since fluorescence microscopy demonstrated localized effects of JD1 on membranes, we investigated whether JD1 altered membranes and/or other cellular structures using transmission electron microscopy (TEM). Cells were treated with $1 \times \text{MIC}_{95}$

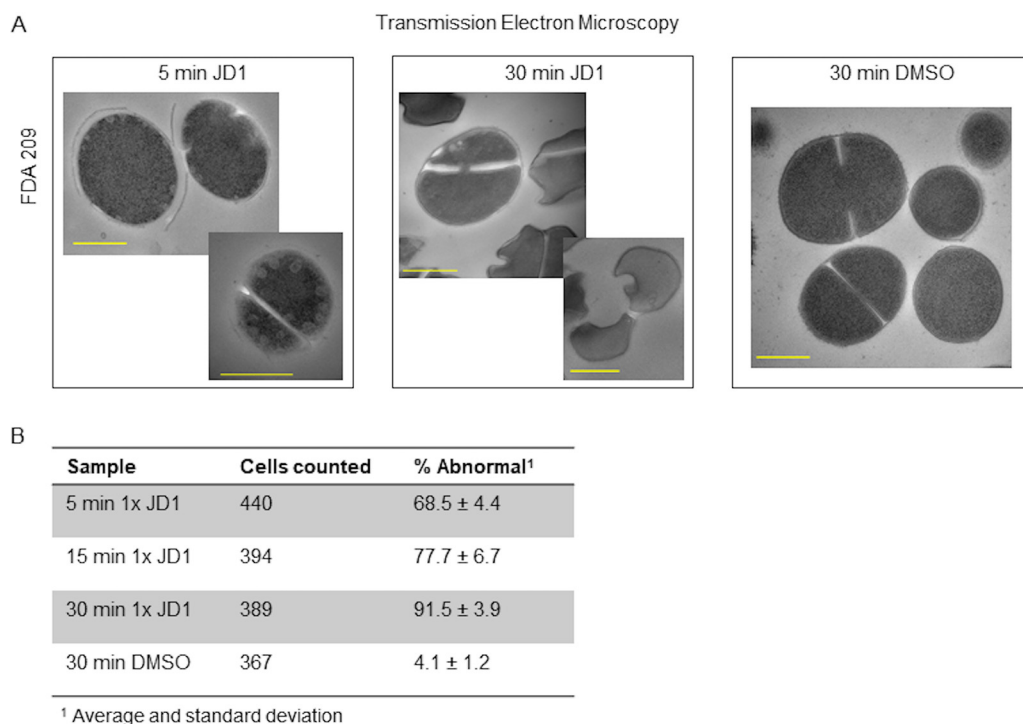


FIG 4 JD1 treatment rapidly leads to abnormal membranous structures in *S. aureus*. (A) Representative transmission electron micrographs of *S. aureus* FDA209 treated with $1 \times \text{MIC}_{95}$ JD1 for 5 and 30 min or with DMSO for 30 min. Bar, 500 nm. Micrographs are representative of biological duplicates. (B) Quantification of TEM images for abnormal *S. aureus* FDA209 cells when treated with $1 \times \text{MIC}_{95}$ JD1 or DMSO. A minimum of 103 cells were counted per treatment, per biological replicate.

JD1 for 5, 15, or 30 min or DMSO for 30 min and imaged by TEM. Within 5 min of JD1 treatment 68.5% of cells displayed aberrant morphology (Fig. 4; Fig. S2). Most aberrant cells contained at least one intracellular membranous vesicle, with some cells containing eight or more per image. After 15 min of treatment, there was a higher percentage of abnormal cells, many with an undulating membrane and/or membrane separation from the peptidoglycan. While 30 min of treatment with $1 \times \text{MIC}_{95}$ JD1 was not bactericidal (Fig. 1), almost all of the cells in these samples were abnormal: the septa of many JD1-treated cells were distorted, and the membrane pulled away from the cell wall (Fig. 4A and B; Fig. S2). These data confirm that treatment with JD1 causes rapid formation of internal membranous blebs and further reveal severe cell division and morphological defects.

JD1 decreases the survival of staphylococcal persister cells in broth. To test whether JD1, like other compounds that target the cell membrane, reduces Gram-positive bacterial persister populations in broth, we established a population of cells with a high percentage of persisters (13, 49). Cultures were grown for 18 h and then treated with DMSO, antibiotics, or a dose range of compound JD1 for 3 or 24 h and then plated for CFU enumeration. Since persister, but not planktonic, cells are resistant to clinical antibiotics such as vancomycin and ciprofloxacin, high doses of these antibiotics were used to ensure that the population of cells being tested were indeed persister cells (11). As expected, in all four strains tested, high doses of vancomycin and ciprofloxacin did not decrease the number of viable cells recovered (Fig. 5A to D). After 24 h of treatment with $2 \times \text{MIC}_{95}$ JD1, *S. aureus* FDA209 persister populations decreased 10-fold and *S. epidermidis* persisters declined 100-fold. Both *S. aureus* USA300 and HG001 persister populations decreased 100-fold after 24 h of treatment with $4 \times \text{MIC}_{95}$ JD1 and *S. epidermidis* persisters decreased 1,000-fold (Fig. 5A to D). These data show that JD1 is particularly potent against persister cells in broth culture.

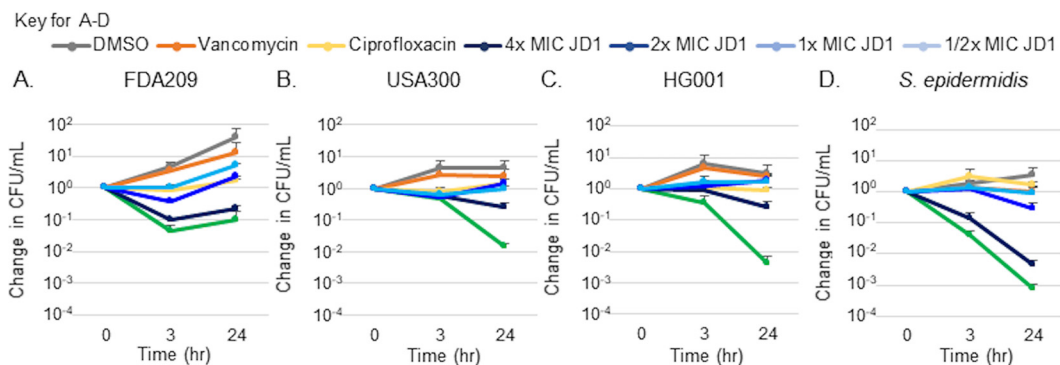


FIG 5 Treatment with JD1 reduced the number of viable staphylococcal persister cells in broth. (A to D) Overnight cultures of the indicated strains were treated at time zero with DMSO, ciprofloxacin (4 $\mu\text{g}/\text{ml}$), vancomycin (10 $\mu\text{g}/\text{ml}$), or the corresponding MIC_{95} of JD1 (Table 1). Cultures were plated for enumeration of CFU at time points indicated. Means and SEM for three biological replicates are shown.

Treatment with JD1 does not inhibit *Staphylococcus* biofilm formation but reduces established biofilms. The bacterial membrane has been posited as an ideal target for preventing and clearing biofilms (24). Since JD1 clearly damages *S. aureus* cell membranes, we established whether this compound inhibits biofilm formation or maintenance. We evaluated biofilm formation by planktonic *S. aureus* over 24 h in the presence of JD1 at subinhibitory concentrations, which were necessary to allow *S. aureus* survival (Fig. 1D). We monitored biofilm mass with crystal violet staining. Both control antibiotics (rifampin and vancomycin) inhibited biofilm formation in some but not all strains tested, and vancomycin promoted biofilm formation in some instances. JD1 treatment slightly inhibited biofilm formation only in *S. epidermidis* and *S. aureus* USA300 and promoted biofilm formation in strain FDA209 (Fig. 6A to D). We also monitored the volume of live and dead cells in biofilms using Syto9 and PI, respectively. Biofilms were imaged with a spinning disc confocal microscope, and volumes were quantified. Rifampin treatment significantly reduced the volume of live and dead cells in *S. aureus* HG001 and *S. epidermidis* biofilms, but JD1 treatment only slightly inhibited the formation of *S. epidermidis* biofilms (Fig. 6E and F). JD1 therefore modestly inhibits biofilm formation in some strains tested.

We next examined whether JD1 disrupts the maintenance of established 1- and 5-day-old biofilms by monitoring mass and volume. We treated biofilms with a range of concentrations of DMSO, vancomycin, rifampin, or JD1 for 18 h. Rifampin reduced day-old biofilms in three of the four *Staphylococcus* strains tested, and vancomycin less so. However, JD1 reduced the 1-day-old biofilm mass of all *Staphylococcus* strains tested as well as or better than rifampin (Fig. 7A to D). JD1 was also at least as potent as rifampin at reducing the volume of live cells at $4\times \text{MIC}_{95}$ in both staphylococcal species (Fig. 7E and F). Volume reconstructions of the imaged biofilms confirmed that *S. aureus* HG001 formed shorter ($\sim 38 \mu\text{m}$) biofilms than *S. epidermidis* ($\sim 80 \mu\text{m}$). Nevertheless, treatment of either strain with JD1 reduced biofilm height by decreasing the volume of live cells, as opposed to decreasing the volume of dead cells (Fig. 7G and H). In addition, the reconstructions of the DMSO controls for *S. aureus* HG001 revealed peaks of biofilm that were diminished by JD1 or rifampin treatment (Fig. 7G). There was no significant JD1 effect on 5-day-old biofilms, with the exception that $8\times \text{MIC}_{95}$ JD1 reduced the mass of *S. aureus* FDA209 (Fig. S3). These data illustrate that JD1 was effective at reducing the mass and cell volume of 1-day-old biofilms in all strains tested as well as or better than antibiotic controls.

JD1 reduces replication and survival of intracellular *S. aureus*. Since intracellular *S. aureus* may be a major cause of reoccurring infections and contribute to the development of antibiotic resistance, we next tested whether JD1 was effective at reducing viable intracellular *S. aureus* with the USA300 strain in both RAW264.7 and HeLa cells (50, 51). As a control, infected cells were treated with vancomycin at a concentration

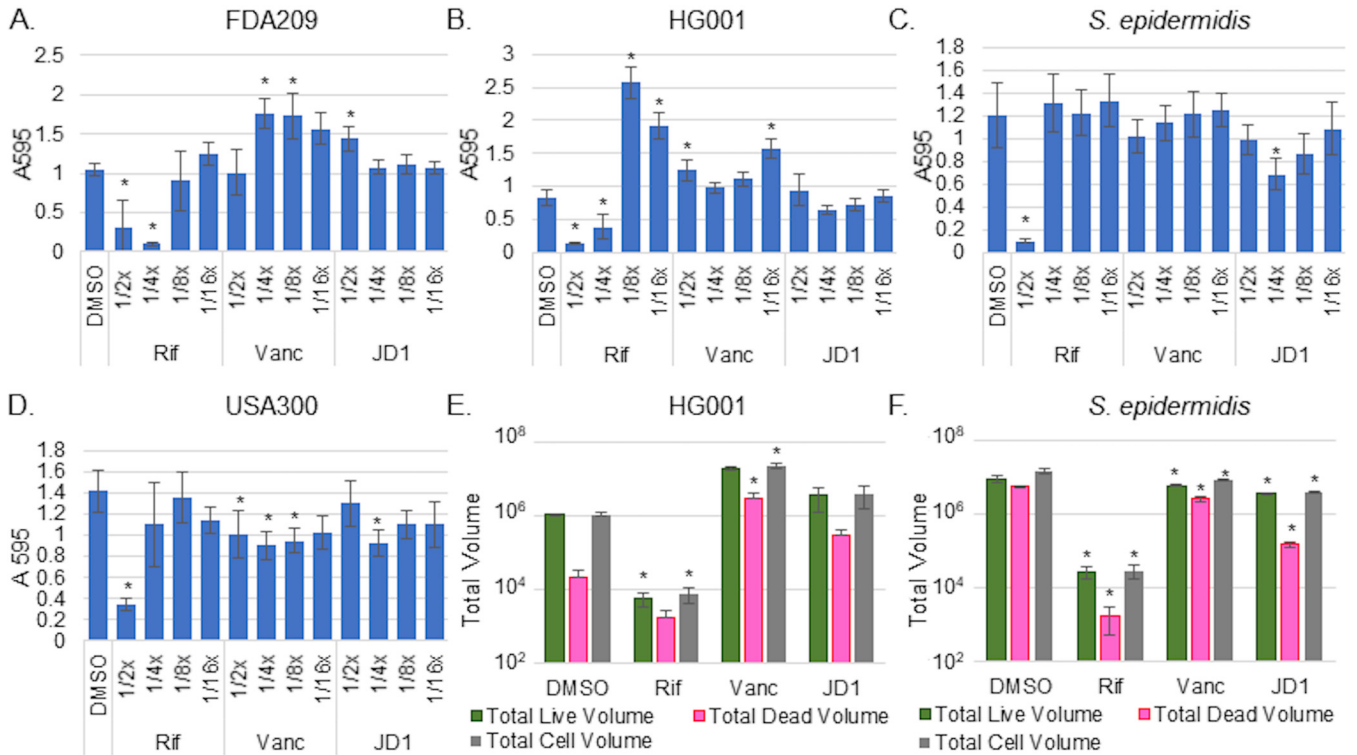


FIG 6 JD1 is minimally effective at inhibiting staphylococcal biofilm formation. Biofilm formation was monitored after 18 h in TSB with subinhibitory concentrations of DMSO, rifampin ($1 \times \text{MIC}_{95} = 0.05 \mu\text{g/ml}$), vancomycin ($1 \times \text{MIC}_{95} = 1 \mu\text{g/ml}$), or JD1. (A to D). Crystal violet staining for accumulated biofilm mass measured at A_{595} . Means and SEM of three biological replicates performed with technical triplicates are shown. (E and F). Biofilms were stained with Syto 9 (live cells) and PI (damaged/dead cells) and imaged with confocal fluorescence microscopy. Volume of live, dead, and total cell volume was calculated (positive volume = positive voxel; 1 voxel = $0.0367 \mu\text{m}^3$). Asterisks indicate P values of ≤ 0.05 as determined by one-way ANOVA compared to DMSO. Panels A to D show means and SEM for three biological replicates performed in triplicate. Panels E and F show means and SDs for one of two biological replicates derived from a minimum of four fields of view.

($25 \mu\text{g/ml}$; $16.83 \mu\text{M}$) within the range found in the blood of patients treated with this last line of defense antibiotic (52). Vancomycin decreased the number of recoverable bacteria less than 10-fold. JD1 treatment decreased the number of recoverable bacteria in both cell types to the limit of detection, with a 50% inhibitory concentration (IC_{50}) of $10.0 \pm 1.1 \mu\text{M}$ in RAW264.7 cells and of $3.6 \pm 1.3 \mu\text{M}$ in HeLa cells (Fig. 8). Thus, JD1 is more potent against *S. aureus* within host cells than in broth culture. Since bacteria within host cells are exposed to lysozyme and other innate immune insults, we tested whether lysosome potentiates JD1 but found no evidence of interaction (Fig. S4). We also examined whether growth in nutrient-limited medium increased the potency of JD1, as host cells often limit pathogen access to nutrients. The MIC_{50} of JD1 in *S. aureus* USA300 under nutrient-limiting conditions was $10.7 \pm 0.6 \mu\text{M}$, compared to $29.1 \pm 2.0 \mu\text{M}$ in LB (Fig. 8C), suggesting that nutrient limitation potentiates JD1. Moreover, at concentrations that are not toxic to host cells (30), JD1 reduced the survival of intracellular *S. aureus* USA300 better than vancomycin.

DISCUSSION

Mechanism of action of JD1 in *Staphylococcus* species. The small molecule JD1 enables the killing of *S. Typhimurium* in macrophages and damages Gram-negative inner membranes when the outer membrane is permeabilized or in strains with loss-of-function mutations in efflux pumps. Here, we examined the effect of JD1 on Gram-positive bacteria, which lack an outer membrane. JD1 was bactericidal in two genera of Gram-positive bacteria and appeared to damage the cell membrane of *S. aureus*. Upon exposure to JD1, the membrane rapidly depolarized, laurdan GP decreased, and intracellular membranous blebs were observed. Within 5 min, barrier function was disrupted and numerous intracellular vesicles had accumulated within a majority of cells.

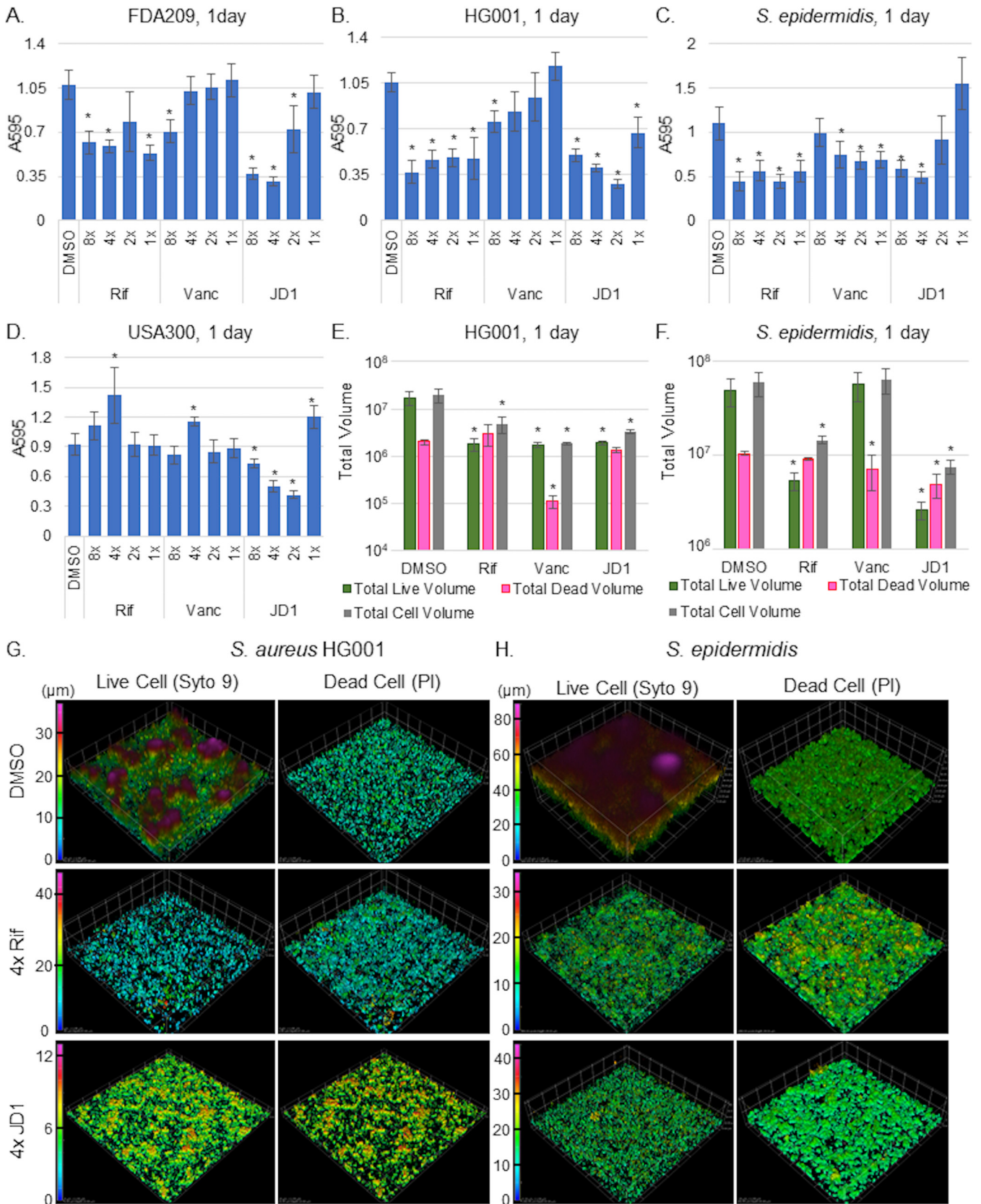


FIG 7 JD1 decreases 1-day-old staphylococcal biofilms. For the indicated strain, biofilms established in TSB for 24 h were treated for 18 h with DMSO, rifampin (1× MIC₉₅ = 0.05 μg/ml), vancomycin (1× MIC₉₅ = 1 μg/ml), or JD1. The remaining biofilm matrix was quantified with crystal violet (A to D), or volume was quantified after Syto9 and PI staining (E and F) as in Fig. 5G and H) Syto9 and PI-stained Z-stacked images were converted to volumes.

(Continued on next page)

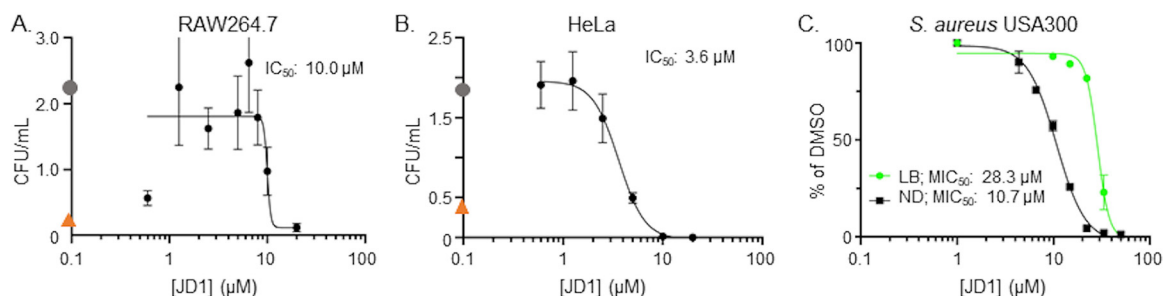


FIG 8 Treatment with JD1 reduces *S. aureus* survival within mammalian cells. (A) RAW 264.7 macrophage-like cells or (B) HeLa cells were infected with *S. aureus* USA300 at MOIs of 0.5 and 2.5, respectively. Cells were treated 2 h after infection with DMSO (gray circle), vancomycin (25 μg/ml; orange triangle), or dilutions of JD1 from 20 μM. After 8 h of infection, cells were lysed and plated for enumeration of CFU. Means and SEM of biological duplicates performed with technical triplicates, each with six dilutions of JD1, are shown. The IC₅₀s are indicated. (C) Dose-response curves monitoring bacterial growth of *S. aureus* USA300 from an OD₆₀₀ of 0.01 in nutrient-depleted (ND) media and LB normalized to growth in 2% DMSO. Means and SEM for at least three biological replicates performed with technical triplicates are shown. All data are from at least biological triplicates for each concentration of JD1. (A and B) Numbers are 10⁵ CFU/ml for A and B.

The rapid changes observed suggest that JD1 affects the arrangement of lipids; decreased laurdan GP is consistent with either or both increased membrane fluidity or the curvature of internal membrane vesicles (45, 47, 53). With longer periods of exposure to JD1, ATP levels and reduction potential declined. JD1 also killed persister cells, reduced the matrix and cell volume of 1-day-old biofilms, and increased the killing of intracellular *S. aureus*. Thus, the cell membrane-damaging activity of JD1 enables this compound to prevent the survival of *S. aureus* grown under conditions germane to infection.

Comparison of JD1 and vancomycin activity against *Staphylococcus* species.

Vancomycin (1449 g/mol) inhibits cell wall biosynthesis and is currently used as a last line of defense drug against methicillin-resistant *S. aureus* (MRSA) (54). Vancomycin is extremely effective at killing *S. aureus* in broth culture, with an MIC₉₅ in LB of ~1 to 2 μg/ml, approximately 15-fold less than that of JD1. However, when difficult-to-treat growth stages are considered, JD1 is more effective than vancomycin (Table 2). Vancomycin was not able to kill staphylococcal persister cells in broth culture, whereas JD1 reduced persisters by as much as 1,000-fold. JD1 was also more effective than vancomycin at reducing 1-day-old staphylococcal biofilms and viable intracellular *S. aureus*. These data underscore the importance of testing compound potency not only in planktonic bacteria but also under infection-relevant growth conditions. In addition, compounds that damage cell membranes may be more useful for treating critical *in vivo* staphylococcal growth stages than clinical antibiotics.

Utility of JD1 for establishing membrane vulnerabilities of Gram-positive bacteria in different growth states. The observation that planktonic cells are vulnerable to membrane-damaging agents such as JD1 is consistent with previous results obtained with other bactericidal small molecules (Table 2). For instance, violacein (343 g/mol), like JD1, disrupts membrane barrier function and causes rapid ATP leakage in planktonic cells (55, 56). In contrast to JD1, neither rhodomlyrtone (443 g/mol) nor reutericyclin (349 g/mol) disrupts barrier function. Rhodomlyrtone, like JD1, causes rapid membrane depolarization (57). Reutericyclin dissipates the pH gradient (58, 59). Thus, planktonic Gram-positive cells are susceptible to multiple kinds of membrane damage.

FIG 7 Legend (Continued)

Volume data were compiled and reconstructed in Nikon Elements Advanced Research software using a color-coded volume display where blue is the bottom, lowest Z-stack and magenta is the highest point for each sample. The scale is in micrometers. Asterisks indicate *P* values of ≤0.05 as determined by one-way ANOVA compared to DMSO. Panels A to D show means and SEM from three biological replicates performed in triplicate. Panels E and F show means and SDs for one of two replicates derived from a minimum of four fields of view. Panels G and H show representative images from the replicate in E and F.

TABLE 2 Comparison of vancomycin and membrane-active small molecules against different types of staphylococcal growth

| Growth state | Relative potency ^a | | | | |
|-------------------------|-------------------------------|------------|-----------|--------------|---------------|
| | JD1 | Vancomycin | Violacein | Rhodomyrtone | Reutericyclin |
| Broth culture | + | +++ | +++ | +++ | ++ |
| Persisters | ++ | – | NA | ++ | NA |
| Biofilms | ++ | + | +++ | ++ | +++ |
| Intracellular infection | +++ | + | NA | + | + |

^aRelative potency of JD1 versus the indicated compounds. The minus sign indicates no detected potency. NA, not applicable (the corresponding experiments were not done or the results were not clear).

The properties of JD1 further reveal the utility of this compound for identifying the vulnerabilities of persister cells, biofilms, and intracellular bacteria (Table 2). Rhodomyrtone, like JD1, probably kills persisters, as it reduces viable cells in a nongrowing culture by 4 orders of magnitude (57). Therefore, the energetics of persister cell membranes are likely susceptible to small molecules. Given that biofilms are inherently difficult to treat, it is encouraging that JD1, rhodomyrtone, violacein, and reutericyclin all have potency against biofilms (23, 60–62). These data indicate that agents with distinct membrane-damaging activities will be useful as tools to clarify the weak points of biofilms. However, whether any of these compounds, like JD1, kill intracellular bacteria remains unknown.

Infection potentiates small-molecule access to Gram-positive bacterial cell membranes. During infection, soluble host defense molecules damage the cell wall of Gram-positive bacteria, likely increasing their sensitivity to compounds. For example, the *S. aureus* USA300 strain is exposed to harsh conditions during replication within the macrophage phagolysosome (50), including various antimicrobial peptides (AMPs), reactive oxygen species (ROS), proteases, lysozyme, low pH, and limited nutrients (63–65). *S. aureus* responds by producing enzymes that detoxify ROS (66, 67), generating ammonia to counter acidification (68), or modifying the membrane and peptidoglycan to resist AMPs and lysozyme (69–71). In HeLa cells, *S. aureus* USA300 escapes the phagosome and replicates in the host cell cytoplasm (72, 73). In this study, we found that *S. aureus* is 2 to 3 times more sensitive to JD1 in HeLa cells with respect to the IC₅₀ and the reduction of viable bacteria than in RAW264.7 cells, possibly reflecting bacterial physiological differences in these two host cell types. Furthermore, *S. aureus* was more sensitive to JD1 in host cells than in LB and had heightened sensitivity to JD1 in nutrient-depleted medium versus LB. These data suggest that nutrient limitation within host cells increases *S. aureus* vulnerability to membrane damage. The multiple environmental stresses to which bacteria are exposed within an animal act in concert to cripple bacteria, and dynamic infection microenvironments are not likely duplicated in any broth culture.

Host membrane toxicity of small membrane-targeting probes. A key question for all membrane-active compounds is whether their activity is specific to bacterial versus mammalian cell membranes. This issue is generally addressed with hit compounds from screens, but the interpretation of results is complicated. First, if membrane-targeting compounds interact with host cell membranes, the much larger volume of host membrane likely dilutes out the compound, reducing the concentration that reaches the bacteria. While mammalian cell cholesterol and neutral lipids appear to protect host cells from JD1 (30), we do not know how much JD1 reaches bacteria in the phagosome. However, since *S. Typhimurium* in macrophages is killed by JD1 at concentrations that are 30-fold lower than that which disrupt host cell membranes, *S. Typhimurium* in phagosomes likely becomes vulnerable to small molecules due to cell envelope damage caused by host innate immunity (30, 74, 75). Both JD1 and rhodomyrtone are probably too toxic for development as therapeutics; they kill cultured cells at concentrations as low as 10 μ M and 1 to 3 μ M, respectively (30, 76). However, analogs of reutericyclin are 12 times less toxic to host cells and still damage bacterial cell

membranes (58), demonstrating that medicinal chemistry efforts may separate compound toxicity from activity.

Conclusions. Collectively, JD1 and the other small molecules described suggest the feasibility of selective targeting of the bacterial cell membrane over host membranes. They also reveal that membrane-active compounds are effective against MDR bacteria and that some are potent against persister cells, biofilms, and intracellular bacteria. The variability in compound potency under different growth conditions and within mammalian cells highlights the importance of identifying and optimizing compounds under conditions relevant to infection. Moreover, the cell membranes of both Gram-negative and Gram-positive bacteria may be useful antibiotic targets for difficult-to-treat infections.

MATERIALS AND METHODS

Bacterial strains. *B. subtilis* (ATCC 6633), *S. aureus* Newman (AH1178), *S. aureus* FDA209 (ATCC 6538), *S. aureus* HG001 (AH2183), *S. aureus* USA300, and *S. epidermidis* 1457 (AH2490) were used in this study.

Media and reagents. Unless otherwise stated, bacteria were grown in lysogeny broth (LB) at 37°C with aeration. JD1 is commercially available (BTB12794; MolPort). To obtain mid-log-phase cells, bacteria were grown overnight in LB, diluted the next morning 1:100 in fresh LB, and then grown to mid-log phase (OD_{600} , 0.4 to 0.6). To test bacterial growth in nutrient-depleted conditions, bacteria were grown in $0.25 \times$ SSM9PR ($0.25 \times$ M9 salts, 0.5 mM $MgSO_4$, 0.25 mM $CaCl_2$, 0.25% glucose, 0.25% Casamino Acids, 0.25 mM thiamine-HCl, 12.5 μ M nicotinamide). The fractional inhibitory concentration indexes (FICIs) for JD1 and novobiocin in *S. Typhimurium* (SL1344) (77) and *E. coli* (K-12) (78) were established in M9 (42 mM Na_2HPO_4 , 22 mM KH_2PO_4 , 18.7 mM NH_4Cl , 8.5 mM NaCl, 0.1% Casamino Acids, 1 μ M $MgSO_4$, 2% glucose) (30) and calculated as follows (79): $(MIC_{DrugA \text{ in combination}}/MIC_{DrugA \text{ alone}}) + (MIC_{DrugB \text{ in combination}}/MIC_{DrugB \text{ alone}})$.

MIC determination. Overnight cultures were diluted in LB to an optical density at 600 nm (OD_{600}) of 0.01 and distributed into polystyrene 96-well flat-bottom plates (Greiner; 655185). Compound was added to the desired final concentration, and the final DMSO concentration never exceeded 2%. Plates were grown at 37°C with shaking for 18 h, and OD_{600} was monitored (BioTek Synergy H1 or BioTek Eon). MICs were defined as the concentration at which 95% of growth was inhibited (determined by OD_{600}) using the curve determined by a variable slope nonlinear regression in GraphPad Prism with a 95% confidence interval.

Growth curves and kill curves. Mid-log-phase cultures were sampled at time zero, and then compound or vehicle control (DMSO) was added. Cultures were incubated at 37°C with agitation. At the time intervals indicated, aliquots were monitored for OD_{600} and plated for CFU enumeration. Data for OD_{600} and CFU/ml were normalized to those at time zero.

Membrane potential assays. Membrane potential was measured using the potentiometric fluorescent probe DiSC₃(5) (Invitrogen). Mid-log-phase cells were diluted to an OD_{600} of 0.4. DiSC₃(5) was added to a final concentration of 2 μ M and the culture was incubated at 37°C in a rotator for 15 min. To remove unincorporated DiSC₃(5) remaining in the medium, cells were captured with vacuum filtration on a 0.45- μ m Metrical membrane filter (Pall), resuspended in fresh LB, and distributed (200 μ l) into black polystyrene 96-well plates (Greiner, 655076). Plates were monitored (excitation wavelength [ex], 650 nm; emission wavelength [em], 680 nm) on a BioTek Synergy H1 plate reader. After baseline fluorescence was recorded, compound was added to the desired final concentration, and measurements were recorded for an additional 30 min. Control wells without bacteria and containing medium with 2 μ M DiSC₃(5) and DMSO had an average RFU of $3,197 \pm 179$. After the addition of $2 \times$, $1 \times$ (30 μ M for *S. aureus* FDA209), or $0.5 \times$ JD1, DiSC₃(5) fluorescence was $191\% \pm 9\%$, $169\% \pm 6.9\%$, and $144\% \pm 3.3\%$ of that in DMSO-treated cells, respectively. These values represent the maximum increase in fluorescence due to compound addition in the presence of DiSC₃(5). Note that with $2 \times$ MIC JD1 in the presence of cells (Fig. 2A), DiSC₃(5) signal increased by approximately 15,000%, dwarfing the percent increase observed without cells present.

Monitoring intracellular pH with BCECF. BCECF-AM (Molecular Probes) was added to mid-log-phase cells in modified LB (LB with 0.1% glucose, 50 mM HEPES, 300 mM KCl [pH 7.0]) to a final concentration of 10 μ M and incubated at 37°C in a rotator for 1 h. Cells were diluted 1:10 and pipetted into a black polystyrene 96-well plate (Greiner; 655076). After 5 min of equilibration, compounds were added and fluorescence (ex, 490 nm/em, 535 nm; ex, 440 nm/em, 535 nm) was monitored every 2.5 min for 20 min using a BioTek Synergy H1 plate reader. BCECF fluorescence was calibrated at 7 pHs between 5.5 and 8 (0.5 pH increments): $pH = pK_a - \log(I_{490}/I_{440})$ (where I_{490} and I_{440} are the fluorescence intensities at 490 and 440 nm, respectively); the pK_a of BCECF is 6.97 (80). During calibration with untreated cells, fluorescent signal did not change in cells incubated in media at pH 5.5. In contrast, signal declined over time in media at pH 8.0, as I_{440} decreased and I_{490} increased. Thus, the decline in signal observed across all treatments likely reflects cell acclimation to pH 7.

Resazurin assays. Mid-log-phase cells (200 μ l per well) were transferred to a black polystyrene 96-well plate (Greiner; 655076) containing compound. Compound was added, and the plate was incubated with shaking. Resazurin (AlamarBlue; Invitrogen) was added to a final concentration of 100 μ g/ml 5 min prior to the indicated time point. The plate was incubated with shaking in the dark at room temperature for 5 min. Fluorescence readings were taken (ex, 570 nm/em, 650 nm) using a BioTek Synergy H1 plate reader.

ATP measurements. Intracellular ATP levels were measured using a BacTiter-Glo microbial cell viability assay (Promega) according to the manufacturer's instructions. Mid-log-phase cells (100 μ l) were added to DMSO, chloramphenicol (32 μ g/ml) (81), or 2 μ l of compound in a black polystyrene 96-well plate (Greiner; 655076) and incubated for 10 or 25 min at 37°C with agitation. Reagent (100 μ l) was added, and samples were incubated in the dark with agitation for 5 min. Luminescence was read on a BioTek Synergy H1 plate reader.

Propidium iodide membrane barrier assays. Compound, DMSO, or SDS (0.5%) was added to mid-log-phase cells to the desired concentration, and cultures were sampled at 0, 5, 10, 15, and 30 min. Five minutes before harvesting, PI [10 μ g/ml] (Life Technologies) was added. Cells were pelleted, washed twice, resuspended in phosphate-buffered saline (PBS), and monitored (ex, 535/em, 617 nm) using a BioTek Synergy H1 plate reader.

Membrane fluidity assays with laurdan. Cells were grown to mid-log phase in LBg (LB with 0.2% glucose). Laurdan (Invitrogen) was added to a final concentration of 10 μ M and incubated at 37°C with rotation for 30 min. Cells were harvested by centrifugation, washed three times, and resuspended in pre-warmed PBSg (PBS with 0.2% glucose). Cells (200 μ l) were transferred to a black polystyrene 96-well plate (Greiner; 655076) and monitored (ex, 360/em, 450 and 500 nm) on a BioTek Synergy H1 plate reader. Baseline fluorescence was recorded for 5 min prior to addition of compound. Fluorescence was recorded for 25 additional minutes. Laurdan generalized polarization (GP) was calculated: $GP = (I_{460} - I_{500}) / (I_{460} + I_{500})$.

Bacterial SR-SIM fluorescence microscopy. Nile red (Sigma-Aldrich) and Hoechst 33342 (Sigma-Aldrich) were added to mid-log-phase cells to a final concentration of 30 μ M and incubated at 37°C for 10 min. For live-cell imaging, cells were harvested by centrifugation at 10,000 $\times g$ for 1 min and resuspended in 100 μ l FluoroBrite Dulbecco's modified Eagle medium (DMEM). Three microliters of cells was deposited onto an agar pad (20% LB, 2% agarose) containing DMSO or 1 \times MIC JD1. Cells were covered with a number 1.5H coverslip and imaged at the indicated times as described below. For fixed-cell imaging, cells were treated with DMSO or 1 \times MIC JD1 for the time indicated. Cells were harvested by centrifugation at 10,000 $\times g$ for 1 min. The supernatant was carefully aspirated off, and the cells were fixed for 10 min in 1 ml of 4% EM-grade paraformaldehyde (PFA; Electron Microscopy Sciences) diluted in PBS. Cells were harvested by centrifugation at 10,000 $\times g$ for 1 min and resuspended in 100 μ l of PBS, and 20 μ l was placed on a number 1.5H glass coverslip. Bio-Rad Frame-Seal incubation chambers (15 by 15 mm, 65 μ l) were adhered to glass slides and filled with 30 μ l of PBS. Coverslips were inverted and adhered to the Frame-Seal chambers, creating a sealed container with 50 μ l of cell suspension. For both live-cell and fixed-cell imaging, slides were imaged in 3D-SIM mode using a Nikon structured illumination superresolution microscope with a 100 \times /1.49 numerical aperture (NA) oil SR Apo TIRF WD 0.12 (mm) objective and/or an iXon X3 EM-CCD 512-by-512 16-bit camera. Standard filter sets were used to capture Hoechst and Nile red emissions, with excitation at 405 and 561 nm, respectively. Nikon Perfect Focus and manual focusing were used to find the best focal plane during acquisition. Images were reconstructed using Nikon Elements SR-SIM analysis software with the default reconstruction parameters.

Electron microscopy. Mid-log cultures were treated with JD1 or DMSO for the stated amount of time and centrifuged at 10,000 $\times g$ for 2 min, and most of the supernatant was removed. Pelleted samples were resuspended in cryoprotectant (150 mM D-mannitol in growth medium) and then centrifuged to a loose pellet, and supernatant was discarded. A few microliters of each pelleted sample was high-pressure frozen using a Wohlwend Compact 02 high-pressure freezer (Technotrade International, Manchester, NH) as described previously (82). Frozen specimens were then freeze-substituted in anhydrous acetone containing 2% osmium tetroxide and 0.2% uranyl acetate and embedded in Epon/Araldite resin. Serial thin sections (60 to 80 nm) were cut using a Leica UCT ultramicrotome. The serial sections were collected on Formvar-coated copper slot grids, poststained with 2% aqueous uranyl acetate followed by Reynold's lead citrate, and imaged using a Tecnai T12 Spirit TEM, operating at 100 kV. Thin sections (80 nm) were cut using a Leica Ultracut UCT microtome and collected onto Formvar-coated copper slot grids. The sections were post-stained with 2% uranyl acetate and Reynold's lead citrate. Samples were imaged in a Tecnai T12 SpiritBT TEM using an AMT charge-coupled device (CCD) camera.

Persister assays. Cultures were grown overnight in Trypticase soy broth (TSB) at 37°C with aeration for 18 h and then divided into samples. Each sample was monitored for enumeration (time zero), and then antibiotic or compound was added to the desired final concentration. Samples were incubated at 37°C with aeration and monitored at 3 and 24 h for enumeration.

Biofilm inhibition assays. Cultures were grown to mid-log phase in TSB and diluted to 4 $\times 10^6$ CFU/ml in TSB, and 200 μ l of this dilution was added to each well of a flat-bottomed polystyrene 96-well (Greiner; 655185) plate; 4 μ l of DMSO, antibiotic, or compound was added to achieve the desired final concentration. Edge wells on the plate were filled with PBS to minimize evaporation of experimental wells. After 24 h of incubation at 37°C with no agitation, the media and planktonic cells were carefully removed, and wells were washed twice with PBS. A multichannel pipette was used for removal of media and subsequent PBS washes.

Biofilm growth and treatment. Cultures were grown to mid-log phase in TSB and diluted to 4 $\times 10^6$ CFU/ml in TSB, and 200 μ l was added to each well of a flat-bottomed polystyrene 96-well (Greiner; 655185) plate (edge wells on the plate were filled with PBS to minimize evaporation of experimental wells). After 24 h of incubation at 37°C without agitation, wells were carefully washed twice with PBS followed by the addition of 200 μ l of TSB containing 4 μ l DMSO, antibiotic, or compound to achieve the desired final concentration. For 5-day biofilm assays, wells were washed and received fresh media daily, and DMSO, antibiotic, or compound was added on day 5. Plates were

incubated at 37°C for 18 h without agitation. Prior to staining, the biofilm was washed twice with PBS to remove nonadherent cells.

Measuring biofilm mass with crystal violet. Plates containing washed biofilms were allowed to air dry; then, 200 μ l of 0.01% crystal violet was added to each well and incubated for 20 min. The biofilms were washed once with deionized (DI) water and air dried. The stained biofilm was resuspended in 200 μ l 70% ethanol, and the A_{595} was measured (BioTek Synergy H1 or BioTek Eon).

Biofilm volume microscopy and analysis. Biofilms were grown as described above, with the following differences. Biofilms were grown in Cellvis 35-mm number 1.5H glass-bottom, 20-mm-well dishes. PBS washes to remove nonadherent cells (cells not attached to the biofilm) were performed with serological pipettes to minimize disruption. Biofilms were stained for 15 min prior to imaging with PI (10 μ g/ml) and Syto9 (3 μ M) resuspended in PBS. The dye solution was gently removed with a pipette, and samples were washed twice with PBS and imaged live (fixation with 4% PFA resulted in a PI-staining artifact). Images were acquired using the Yokogawa CellVoyager CV1000 confocal scanner system with a 40 \times /0.6 NA working distance 2.7 to 4.0 (mm) objective, a MicroLens-enhanced Nipkow disk scanner with a pinhole size of 50 μ m, and a Hamamatsu Photonics ImagEM X2 EM-CCD C9100-14 camera with high-resolution 16-bit format. Prior to image acquisition, the Z range of each biofilm was determined by manually establishing the top and bottom, and the z-step size was set to 1 μ m to simplify volume analysis (conversion between volume and voxels). Images were acquired in two color channels: ex/em for Syto9 and PI at 488 nm_{525/50} and 561 nm_{617/73}, respectively. A minimum of eight randomly selected fields of view were acquired, and at least four images were used for analysis.

Images were imported into MATLAB R2020b as multidimensional tiff stacks and processed as volume data using a custom script designed to store all results in a data structure for user review. Otsu's method was used instead of manual thresholding due to different levels of background signals across samples (83). Three-dimensional (3D) binary masks were created to extract Syto9 and PI foreground signals from background (83). The total volume for each of the two channels was quantified as the summation of voxels identified above the threshold per channel. The total number of voxels was converted to total volume (1 voxel = 0.0367 μ m³) using the metadata. Selected volumes were reconstructed in Nikon Elements Advanced Research software using thresholds determined by Otsu's method (from the MATLAB script) to provide a color-coded quantitative volume display based on depth in micrometers.

Intracellular infection assays. RAW 264.7 (TIB-71) macrophages (5×10^4 macrophages in 100 μ l of complete DMEM) were seeded in 96-well tissue culture plates (Greiner; 655180) and were incubated at 37°C with 5% CO₂. For experiments performed with HeLa cells (ATCC CCL-2), 1×10^4 cells were seeded. *S. aureus* USA300 was grown overnight in TSB, subcultured to an OD₆₀₀ of 0.4 in TSB, regrown to an OD₆₀₀ of 0.6, and diluted to a final concentration of 5×10^5 CFU/ml in complete DMEM. Twenty-four hours after seeding, 50 μ l of bacterial culture was added to each cell culture well, an approximate multiplicity of infection (MOI) of 0.5 bacterium to one cell for RAW 264.7 cells and 2.5 bacteria to one HeLa cell. Plates were centrifuged at 500 \times g for 2 min to synchronize the infection. Thirty or 45 min (for RAW 264.7 or HeLa cells, respectively) after bacterial addition, wells were washed once with PBS, DMEM containing 100 μ g/ml gentamicin (Sigma-Aldrich) was added, and cells were incubated for 90 min. Wells were washed twice with PBS. Complete DMEM was added to the wells, followed by 1 μ l of JD1, vancomycin, or vehicle control to the stated final concentration. The highest concentration of JD1 tested was 20 μ M, because higher concentrations were toxic to cells (30). IC₅₀s and 95% confidence intervals were determined using a variable slope nonlinear regression in GraphPad Prism.

Data availability. MATLAB scripts are freely available via the MATLAB file exchange and GitHub (J.L.J.Q.).

SUPPLEMENTAL MATERIAL

Supplemental material is available online only.

FIG S1, TIF file, 0.3 MB.

FIG S2, TIF file, 0.4 MB.

FIG S3, TIF file, 0.05 MB.

FIG S4, TIF file, 0.02 MB.

ACKNOWLEDGMENTS

We appreciate all the members of the Detweiler laboratory for insightful discussions and technical help. We are grateful to D. Evans, C. Ewing, T. Nagy, and J. Villanueva for comments on the manuscript. We thank the MCDB Light Microscopy Facility at the University of Colorado Boulder and in particular J. Orth for expert guidance. Additionally, we thank Leica for allowing use of their demonstration microscope. We also thank the University of Colorado Boulder Electron Microscopy Services Core Facility, especially G. Morgan for sample preparation and E. O'Toole for imaging of samples. Finally, we thank the A. Horswill lab for providing *S. aureus* and *S. epidermidis* strains. Publication of this article was funded by the University of Colorado Boulder Libraries Open Access Fund.

This work was supported by NIH grants AI121365 (C.S.D.) and AI151979 (C.S.D.). The funders had no role in study design, data collection and interpretation, or the decision to submit the work for publication.

REFERENCES

- Theuretzbacher U, Gottwalt S, Beyer P, Butler M, Czaplowski L, Lienhardt C, Moja L, Paul M, Paulin S, Rex JH, Silver LL, Spigelman M, Thwaites GE, Paccard J-P, Harbarth S. 2019. Analysis of the clinical antibacterial and antituberculosis pipeline. *Lancet Infect Dis* 19:e40–e50. [https://doi.org/10.1016/S1473-3099\(18\)30513-9](https://doi.org/10.1016/S1473-3099(18)30513-9).
- Pernodet JL, Fish S, Blondelet-Rouault MH, Cundliffe E. 1996. The macrolide-lincosamide-streptogramin B resistance phenotypes characterized by using a specifically deleted, antibiotic-sensitive strain of *Streptomyces lividans*. *Antimicrob Agents Chemother* 40:581–585. <https://doi.org/10.1128/AAC.40.3.581>.
- Tran TB, Velkov T, Nation RL, Forrest A, Tsuji BT, Bergen PJ, Li J. 2016. Pharmacokinetics/pharmacodynamics of colistin and polymyxin B: are we there yet? *Int J Antimicrob Agents* 48:592–597. <https://doi.org/10.1016/j.ijantimicag.2016.09.010>.
- Bruniera FR, Ferreira FM, Savioli LRM, Bacci MR, Feder D, Azzalis LA, Campos Junqueira VB, Fonseca FLA. 2015. The use of vancomycin with its therapeutic and adverse effects: a review. *Eur Rev Med Pharmacol Sci* 19: 694–700.
- Drown BS, Hergenrother PJ. 2018. Going on offense against the gram-negative defense. *Proc Natl Acad Sci U S A* 115:6530–6532. <https://doi.org/10.1073/pnas.1807278115>.
- Ricci V, Blair JMA, Piddock LJV. 2014. RamA, which controls expression of the MDR efflux pump AcrAB-TolC, is regulated by the Ion protease. *J Antimicrob Chemother* 69:643–650. <https://doi.org/10.1093/jac/dkt432>.
- Nikaido H. 1996. Multidrug efflux pumps of gram-negative bacteria. *J Bacteriol* 178:5853–5859. <https://doi.org/10.1128/jb.178.20.5853-5859.1996>.
- Buckley AM, Webber MA, Cooles S, Randall LP, La Ragione RM, Woodward MJ, Piddock LJV. 2006. The AcrAB-TolC efflux system of *Salmonella enterica* serovar Typhimurium plays a role in pathogenesis. *Cell Microbiol* 8: 847–856. <https://doi.org/10.1111/j.1462-5822.2005.00671.x>.
- Blair JMA, La Ragione RM, Woodward MJ, Piddock LJV. 2009. Periplasmic adaptor protein AcrA has a distinct role in the antibiotic resistance and virulence of *Salmonella enterica* serovar Typhimurium. *J Antimicrob Chemother* 64:965–972. <https://doi.org/10.1093/jac/dkp311>.
- Balaban NQ, Helaine S, Lewis K, Ackermann M, Aldridge B, Andersson DI, Brynildsen MP, Bumann D, Camilli A, Collins JJ, Dehio C, Fortune S, Ghigo J-M, Hardt W-D, Harms A, Heinemann M, Hung DT, Jenal U, Levin BR, Michiels J, Storz G, Tan M-W, Tenson T, Van Melderen L, Zinkernagel A. 2019. Definitions and guidelines for research on antibiotic persistence. *Nat Rev Microbiol* 17:441–448. <https://doi.org/10.1038/s41579-019-0196-3>.
- Conlon BP, Rowe SE, Gandt AB, Nuxoll AS, Donegan NP, Zalis EA, Clair G, Adkins JN, Cheung AL, Lewis K. 2016. Persister formation in *Staphylococcus aureus* is associated with ATP depletion. *Nat Microbiol* 1:16051. <https://doi.org/10.1038/nmicrobiol.2016.51>.
- Peyrusson F, Varet H, Nguyen TK, Legendre R, Sismeiro O, Coppée J-Y, Wolz C, Tenson T, Van Bambeke F. 2020. Intracellular *Staphylococcus aureus* persists upon antibiotic exposure. *Nat Commun* 11:2200. <https://doi.org/10.1038/s41467-020-15966-7>.
- Keren I, Kaldalu N, Spoering A, Wang Y, Lewis K. 2004. Persister cells and tolerance to antimicrobials. *FEMS Microbiol Lett* 230:13–18. [https://doi.org/10.1016/S0378-1097\(03\)00856-5](https://doi.org/10.1016/S0378-1097(03)00856-5).
- Pontes MH, Groisman EA. 2019. Slow growth determines nonheritable antibiotic resistance in *Salmonella enterica*. *Sci Signal* 12:eaax3938. <https://doi.org/10.1126/scisignal.aax3938>.
- Lewis K. 2010. Persister Cells. *Annu Rev Microbiol* 64:357–372. <https://doi.org/10.1146/annurev.micro.112408.134306>.
- Yang S, Hay ID, Cameron DR, Speir M, Cui B, Su F, Peleg AY, Lithgow T, Deighton MA, Qu Y. 2015. Antibiotic regimen based on population analysis of residing persister cells eradicates *Staphylococcus epidermidis* biofilms. *Sci Rep* 5:18578. <https://doi.org/10.1038/srep18578>.
- Schilcher K, Horswill AR. 2020. Staphylococcal biofilm development: structure, regulation, and treatment strategies. *Microbiol Mol Biol Rev* 84: e0026-19. <https://doi.org/10.1128/MMBR.00026-19>.
- Rogers DE. 1956. Studies on bacteremia. *J Exp Med* 103:713–742. <https://doi.org/10.1084/jem.103.6.713>.
- Kapral FA, Shayegani MG. 1959. Intracellular survival of staphylococci. *J Exp Med* 110:123–138. <https://doi.org/10.1084/jem.110.1.123>.
- Watkins KE, Unnikrishnan M. 2020. Evasion of host defenses by intracellular *Staphylococcus aureus*. *Adv Appl Microbiol* 112:105–141. <https://doi.org/10.1016/bs.aambs.2020.05.001>.
- Kamaruzzaman NF, Kendall S, Good L. 2017. Targeting the hard to reach: challenges and novel strategies in the treatment of intracellular bacterial infections. *Br J Pharmacol* 174:2225–2236. <https://doi.org/10.1111/bph.13664>.
- Abed N, Couvreur P. 2014. Nanocarriers for antibiotics: a promising solution to treat intracellular bacterial infections. *Int J Antimicrob Agents* 43: 485–496. <https://doi.org/10.1016/j.ijantimicag.2014.02.009>.
- Hurdle JG, O'Neill AJ, Chopra I, Lee RE. 2011. Targeting bacterial membrane function: an underexploited mechanism for treating persistent infections. *Nat Rev Microbiol* 9:62–75. <https://doi.org/10.1038/nrmicro2474>.
- Herzog IM, Fridman M. 2014. Design and synthesis of membrane-targeting antibiotics: from peptides- to aminosugar-based antimicrobial cationic amphiphiles. *Med Chem Commun (Camb)* 5:1014–1026. <https://doi.org/10.1039/C4MD00012A>.
- Epanand RM, Walker C, Epanand RF, Magarvey NA. 2016. Molecular mechanisms of membrane targeting antibiotics. *Biochim Biophys Acta* 1858: 980–987. <https://doi.org/10.1016/j.bbamem.2015.10.018>.
- Dias C, Rauter AP. 2019. Membrane-targeting antibiotics: recent developments outside the peptide space. *Future Med Chem* 11:211–228. <https://doi.org/10.4155/fmc-2018-0254>.
- Shaw N, Heatherington K, Baddiley J. 1968. The glycolipids of *Lactobacillus casei* A.T.C.C. 7469. *Biochem J* 107:491–496. <https://doi.org/10.1042/bj1070491>.
- Short SA, White DC. 1970. Metabolism of the glycosyl diglycerides and phosphatidylglucose of *Staphylococcus aureus*. *J Bacteriol* 104:126–132. <https://doi.org/10.1128/jb.104.1.126-132.1970>.
- Sohlenkamp C, Geiger O. 2016. Bacterial membrane lipids: diversity in structures and pathways. *FEMS Microbiol Rev* 40:133–159. <https://doi.org/10.1093/femsre/fuv008>.
- Dombach JL, Quintana JJJ, Nagy TA, Wan C, Crooks AL, Yu H, Su C-C, Yu EW, Shen J, Detweiler CS. 2020. A small molecule that mitigates bacterial infection disrupts Gram-negative cell membranes and is inhibited by cholesterol and neutral lipids. *PLoS Pathog* 16:e1009119. <https://doi.org/10.1371/journal.ppat.1009119>.
- Makarova O, Johnston P, Walther B, Rolff J, Roesler U. 2017. Complete genome sequence of the disinfectant susceptibility testing reference strain *Staphylococcus aureus* subsp. *aureus* ATCC 6538. *Genome Announc* 5: e00293-17. <https://doi.org/10.1128/genomeA.00293-17>.
- Myers GE, McCready RGL. 1963. Adverse effect of ammonium salts on the antibacterial activity of paraformaldehyde solutions. *Appl Microbiol* 11: 357–361. <https://doi.org/10.1128/am.11.4.357-361.1963>.
- McLeod JR, Harvey PA, Detweiler CS. 2021. An oral fluorouracil prodrug, capecitabine, mitigates a Gram-positive systemic infection in mice. *Microbiol Spectr* 9:e0027521. <https://doi.org/10.1128/Spectrum.00275-21>.
- Nagel M, Reuter T, Jansen A, Szekat C, Bierbaum G. 2011. Influence of ciprofloxacin and vancomycin on mutation rate and transposition of IS256 in *Staphylococcus aureus*. *Int J Med Microbiol* 301:229–236. <https://doi.org/10.1016/j.ijmm.2010.08.021>.
- Herbert S, Ziebandt A-K, Ohlsen K, Schäfer T, Hecker M, Albrecht D, Novick R, Götz F. 2010. Repair of global regulators in *Staphylococcus aureus* 8325 and comparative analysis with other clinical isolates. *Infect Immun* 78:2877–2889. <https://doi.org/10.1128/IAI.00088-10>.
- Galac MR, Stam J, Maybank R, Hinkle M, Mack D, Rohde H, Roth AL, Fey PD. 2017. Complete genome sequence of *Staphylococcus epidermidis* 1457. *Genome Announc* 5:e00450-17. <https://doi.org/10.1128/genomeA.00450-17>.
- Farha MA, Verschoor CP, Bowdish D, Brown ED. 2013. Collapsing the proton motive force to identify synergistic combinations against *Staphylococcus aureus*. *Chem Biol* 20:1168–1178. <https://doi.org/10.1016/j.chembiol.2013.07.006>.

38. Waggoner AS. 1979. Dye indicators of membrane potential. *Annu Rev Biophys Bioeng* 8:47–68. <https://doi.org/10.1146/annurev.bb.08.060179.000403>.
39. Müller A, Wenzel M, Strahl H, Grein F, Saaki TNV, Kohl B, Siersma T, Bandow JE, Sahl H-G, Schneider T, Hamoen LW. 2016. Daptomycin inhibits cell envelope synthesis by interfering with fluid membrane microdomains. *Proc Natl Acad Sci U S A* 113:E7077–E7086. <https://doi.org/10.1073/pnas.1611173113>.
40. Clementi EA, Marks LR, Roche-Håkansson H, Håkansson AP. 2014. Monitoring changes in membrane polarity, membrane integrity, and intracellular ion concentrations in *Streptococcus pneumoniae* using fluorescent dyes. *J Vis Exp* 2014:e51008. <https://doi.org/10.3791/51008>.
41. Czekanska EM. 2011. Assessment of cell proliferation with resazurin-based fluorescent dye. *Methods Mol Biol* 740:27–32. https://doi.org/10.1007/978-1-61779-108-6_5.
42. Lande MB, Donovan JM, Zeidel ML. 1995. The relationship between membrane fluidity and permeabilities to water, solutes, ammonia, and protons. *J Gen Physiol* 106:67–84. <https://doi.org/10.1085/jgp.106.1.67>.
43. Rössignol M, Uso T, Thomas P. 1985. Relationship between fluidity and ionic permeability of bilayers from natural mixtures of phospholipids. *J Membr Biol* 87:269–275. <https://doi.org/10.1007/BF01871227>.
44. Cruzeiro-Hansson L, Mouritsen OG. 1988. Passive ion permeability of lipid membranes modelled via lipid-domain interfacial area. *Biochim Biophys Acta* 944:63–72. [https://doi.org/10.1016/0005-2736\(88\)90316-1](https://doi.org/10.1016/0005-2736(88)90316-1).
45. Scheinplug K, Krylova O, Strahl H. 2017. Measurement of cell membrane fluidity by Laurdan GP: fluorescence spectroscopy and microscopy. *Methods Mol Biol* 1520:159–174. https://doi.org/10.1007/978-1-4939-6634-9_10.
46. Parasassi T, De Stasio G, Ravagnan G, Rusch RM, Gratton E. 1991. Quantitation of lipid phases in phospholipid vesicles by the generalized polarization of laurdan fluorescence. *Biophys J* 60:179–189. [https://doi.org/10.1016/S0006-3495\(91\)82041-0](https://doi.org/10.1016/S0006-3495(91)82041-0).
47. Zhang Y-L, Frangos JA, Chachivivilis M. 2006. Laurdan fluorescence senses mechanical strain in the lipid bilayer membrane. *Biochem Biophys Res Commun* 347:838–841. <https://doi.org/10.1016/j.bbrc.2006.06.152>.
48. Yano T, Miyahara Y, Morii N, Okano T, Kubota H. 2016. Pentanol and benzyl alcohol attack bacterial surface structures differently. *Appl Environ Microbiol* 82:402–408. <https://doi.org/10.1128/AEM.02515-15>.
49. Allison KR, Brynildsen MP, Collins JJ. 2011. Metabolite-enabled eradication of bacterial persisters by aminoglycosides. *Nature* 473:216–220. <https://doi.org/10.1038/nature10069>.
50. Flannagan RS, Heit B, Heinrichs DE. 2016. Intracellular replication of *Staphylococcus aureus* in mature phagolysosomes in macrophages precedes host cell death, and bacterial escape and dissemination. *Cell Microbiol* 18:514–535. <https://doi.org/10.1111/cmi.12527>.
51. Das S, Lindemann C, Young BC, Muller J, Österreich B, Ternette N, Winkler A-C, Paprotka K, Reinhardt R, Förstner KU, Allen E, Flaxman A, Yamaguchi Y, Rollier CS, van Diemen P, Blättner S, Remmele CW, Selle M, Ditttrich M, Müller T, Vogel J, Ohlsen K, Crook DW, Massey R, Wilson DJ, Rudel T, Wyllie DH, Fraunholz MJ. 2016. Natural mutations in a *Staphylococcus aureus* virulence regulator attenuate cytotoxicity but permit bacteremia and abscess formation. *Proc Natl Acad Sci U S A* 113:E3101–E3110. <https://doi.org/10.1073/pnas.1520255113>.
52. Martin JH, Norris R, Barras M, Roberts J, Morris R, Doogue M. 2010. Therapeutic monitoring of vancomycin in adult patients: a consensus review of the American Society of Health-System Pharmacists, the Infectious Diseases Society of America, and the Society of Infectious Diseases Pharmacists. *Clin Biochem Rev* 31:21–24.
53. Parasassi T, Gratton E. 1995. Membrane lipid domains and dynamics as detected by laurdan fluorescence. *J Fluoresc* 5:59–69. <https://doi.org/10.1007/BF00718783>.
54. Jovetic S, Zhu Y, Marcone GL, Marinelli F, Tramper J. 2010. β -Lactam and glycopeptide antibiotics: first and last line of defense? *Trends Biotechnol* 28:596–604. <https://doi.org/10.1016/j.tibtech.2010.09.004>.
55. Cauz ACG, Carretero GPB, Saraiva GKV, Park P, Mortara L, Cuccovia IM, Brocchi M, Gueiros-Filho FJ. 2019. Violacein targets the cytoplasmic membrane of bacteria. *ACS Infect Dis* 5:539–549. <https://doi.org/10.1021/acscinfecdis.8b00245>.
56. Subramaniam S, Ravi V, Sivasubramanian A. 2014. Synergistic antimicrobial profiling of violacein with commercial antibiotics against pathogenic micro-organisms. *Pharm Biol* 52:86–90. <https://doi.org/10.3109/13880209.2013.815634>.
57. Saeloh D, Tipmanee V, Jim KK, Dekker MP, Bitter W, Voravuthikunchai SP, Wenzel M, Hamoen LW. 2018. The novel antibiotic rhodomycinone traps membrane proteins in vesicles with increased fluidity. *PLoS Pathog* 14:e1006876. <https://doi.org/10.1371/journal.ppat.1006876>.
58. Cherian PT, Wu X, Maddox MM, Singh AP, Lee RE, Hurdle JG. 2014. Chemical modulation of the biological activity of reutericyclin: a membrane-active antibiotic from *Lactobacillus reuteri*. *Sci Rep* 4:4721. <https://doi.org/10.1038/srep04721>.
59. Gänzle MG, Vogel RF. 2003. Studies on the mode of action of reutericyclin. *Appl Environ Microbiol* 69:1305–1307. <https://doi.org/10.1128/AEM.69.2.1305-1307.2003>.
60. Saising J, Ongsakul M, Voravuthikunchai SP. 2011. Rhodomycinone (Aiton) Hassk. ethanol extract and rhodomycinone: a potential strategy for the treatment of biofilm-forming staphylococci. *J Med Microbiol* 60:1793–1800. <https://doi.org/10.1099/jmm.0.033092-0>.
61. Dodou HV, Batista AHM, Medeiros SC, Sales GWP, Rodrigues ML, Pereira PIO, Nogueira PCN, Silveira ER, Grangeiro TB, Nogueira NAP. 2020. Violacein antimicrobial activity on *Staphylococcus epidermidis* biofilm. *Nat Prod Res* 34:3414–3417. <https://doi.org/10.1080/14786419.2019.1569654>.
62. Hurdle JG, Yendapally R, Sun D, Lee RE. 2009. Evaluation of analogs of reutericyclin as prospective candidates for treatment of staphylococcal skin infections. *Antimicrob Agents Chemother* 53:4028–4031. <https://doi.org/10.1128/AAC.00457-09>.
63. Prost LR, Miller SI. 2008. The salmonellae PhoQ sensor: mechanisms of detection of phagosomal signals. *Cell Microbiol* 10:576–582. <https://doi.org/10.1111/j.1462-5822.2007.01111.x>.
64. Pucciarelli MG, García-Del Portillo F. 2017. Salmonella intracellular lifestyles and their impact on host-to-host transmission. *Microbiol Spectr* 5:MTBP-0009-2016. <https://doi.org/10.1128/microbiolspec.MTBP-0009-2016>.
65. Fairn GD, Grinstein S. 2012. How nascent phagosomes mature to become phagolysosomes. *Trends Immunol* 33:397–405. <https://doi.org/10.1016/j.it.2012.03.003>.
66. Cosgrove K, Coutts G, Jonsson I-M, Tarkowski A, Kokai-Kun JF, Mond JJ, Foster SJ. 2007. Catalase (KatA) and alkyl hydroperoxide reductase (AhpC) have compensatory roles in peroxide stress resistance and are required for survival, persistence, and nasal colonization in *Staphylococcus aureus*. *J Bacteriol* 189:1025–1035. <https://doi.org/10.1128/JB.01524-06>.
67. Karavolos MH, Horsburgh MJ, Ingham E, Foster SJ. 2003. Role and regulation of the superoxide dismutases of *Staphylococcus aureus*. *Microbiology (Reading)* 149:2749–2758. <https://doi.org/10.1099/mic.0.26353-0>.
68. Weinrick B, Dunman PM, McAleese F, Murphy E, Projan SJ, Fang Y, Novick RP. 2004. Effect of mild acid on gene expression in *Staphylococcus aureus*. *J Bacteriol* 186:8407–8423. <https://doi.org/10.1128/JB.186.24.8407-8423.2004>.
69. Bera A, Herbert S, Jakob A, Vollmer W, Götz F. 2005. Why are pathogenic staphylococci so lysozyme resistant? The peptidoglycan O-acetyltransferase OatA is the major determinant for lysozyme resistance of *Staphylococcus aureus*. *Mol Microbiol* 55:778–787. <https://doi.org/10.1111/j.1365-2958.2004.04446.x>.
70. Peschel A, Otto M, Jack RW, Kalbacher H, Jung G, Götz F. 1999. Inactivation of the *dlt* operon in *Staphylococcus aureus* confers sensitivity to defensins, protegrins, and other antimicrobial peptides. *J Biol Chem* 274:8405–8410. <https://doi.org/10.1074/jbc.274.13.8405>.
71. Peschel A, Jack RW, Otto M, Collins LV, Staubitz P, Nicholson G, Kalbacher H, Nieuwenhuizen WF, Jung G, Tarkowski A, van Kessel KP, van Strijp JA. 2001. *Staphylococcus aureus* resistance to human defensins and evasion of neutrophil killing via the novel virulence factor Mprf is based on modification of membrane lipids with l-lysine. *J Exp Med* 193:1067–1076. <https://doi.org/10.1084/jem.193.9.1067>.
72. Giese B, Glowinski F, Paprotka K, Dittmann S, Steiner T, Sinha B, Fraunholz MJ. 2011. Expression of δ -toxin by *Staphylococcus aureus* mediates escape from phago-endosomes of human epithelial and endothelial cells in the presence of β -toxin. *Cell Microbiol* 13:316–329. <https://doi.org/10.1111/j.1462-5822.2010.01538.x>.
73. Grosz M, Kolter J, Paprotka K, Winkler A-C, Schäfer D, Chatterjee SS, Geiger T, Wolz C, Ohlsen K, Otto M, Rudel T, Sinha B, Fraunholz M. 2014. Cytoplasmic replication of *Staphylococcus aureus* upon phagosomal escape triggered by phenol-soluble modulins α . *Cell Microbiol* 16:451–465. <https://doi.org/10.1111/cmi.12233>.
74. Sakoulas G, Kumaraswamy M, Kousha A, Nizet V. 2017. Interaction of antibiotics with innate host defense factors against *Salmonella enterica* serotype Newport. *mSphere* 2:e00410-17. <https://doi.org/10.1128/mSphere.00410-17>.
75. Nagy TA, Crooks AL, Quintana JLJ, Detweiler CS. 2020. Clofazimine reduces the survival of *Salmonella enterica* in macrophages and mice. *ACS Infect Dis* 6:1238–1249. <https://doi.org/10.1021/acscinfecdis.0c00023>.

76. Saising J, Nguyen M-T, Härtner T, Ebner P, Al Mamun Bhuyan A, Berscheid A, Muehlenkamp M, Schäkermann S, Kumari N, Maier ME, Voravuthikunchai SP, Bandow J, Lang F, Brötz-Oesterheld H, Götz F. 2018. Rhodomyrone (Rom) is a membrane-active compound. *Biochim Biophys Acta Biomembr* 1860:1114–1124. <https://doi.org/10.1016/j.bbamem.2018.01.011>.
77. Hoiseth SK, Stocker BA. 1981. Aromatic-dependent *Salmonella* Typhimurium are non-virulent and effective as live vaccines. *Nature* 291:238–239. <https://doi.org/10.1038/291238a0>.
78. Lederberg J. 1947. Gene recombination and linked segregations in *Escherichia coli*. *Genetics* 32:505–525. <https://doi.org/10.1093/genetics/32.5.505>.
79. Hall MJ, Middleton RF, Westmacott D. 1983. The fractional inhibitory concentration (FIC) index as a measure of synergy. *J Antimicrob Chemother* 11:427–433. <https://doi.org/10.1093/jac/11.5.427>.
80. James-Kracke MR. 1992. Quick and accurate method to convert BCECF fluorescence to pH: calibration in three different types of cell preparations. *J Cell Physiol* 151:596–603. <https://doi.org/10.1002/jcp.1041510320>.
81. Lobritz MA, Belenky P, Porter CBM, Gutierrez A, Yang JH, Schwarz EG, Dwyer DJ, Khalil AS, Collins JJ. 2015. Antibiotic efficacy is linked to bacterial cellular respiration. *Proc Natl Acad Sci U S A* 112:8173–8180. <https://doi.org/10.1073/pnas.1509743112>.
82. Giddings TH, Jr, Morpew M, McIntosh JR. 2017. Preparing fission yeast for electron microscopy. *Cold Spring Harb Protoc* 2017. <https://doi.org/10.1101/pdb.prot091314>.
83. Sommerfeld Ross S, Tu MH, Falsetta ML, Ketterer MR, Kiedrowski MR, Horswill AR, Apicella MA, Reinhardt JM, Fiegel J. 2014. Quantification of confocal images of biofilms grown on irregular surfaces. *J Microbiol Methods* 100:111–120. <https://doi.org/10.1016/j.mimet.2014.02.020>.